Impact of the Hole Transport Layer on the Charge Extraction of Ruddlesden-Popper Perovskite Solar Cells

Wang, Qingqian; Shao, Shuyan; Xu, Bowei; Duim, Herman; Dong, Jingjin; Adjokatse, Sampson; Portale, Giuseppe; Hou, Jianhui; Saba, Michele; Loi, Maria A

Published in:
ACS Applied Materials & Interfaces

DOI:
10.1021/acsami.0c05290

Publication date:
2020

ACS APPLIED MATERIALS & INTERFACES

www.acsami.org

Research Article

Impact of the Hole Transport Layer on the Charge Extraction of Ruddlesden–Popper Perovskite Solar Cells

Qingqian Wang, Shuyan Shao,* Bowei Xu, Herman Duim, Jingjin Dong, Sampson Adjokatse, Giuseppe Portale, Jianhui Hou, Michele Saba, and Maria A. Loi*

Cite This: *ACS Appl. Mater. Interfaces* 2020, 12, 29505–29512

Read Online

ACCESS | Metrics & More | Article Recommendations | Supporting Information

ABSTRACT: Recent works demonstrate that polyelectrolytes as a hole transport layer (HTL) offers superior performance in Ruddlesden–Popper perovskite solar cells (RPPSCs) compared to poly(3,4-ethylenedioxythiophene) polystyrene sulfonate (PEDOT:PSS). The factors contributing to such improvement need to be systematically investigated. To achieve this, we have systematically investigated how the two HTLs affect the morphology, crystallinity, and orientation of the Ruddlesden–Popper perovskite (RPP) films as well as the charge extraction of the RPPSCs. PEDOT:PSS as a HTL leads to RPP films of low crystallinity and with a number of large pinholes. These factors lead to poor charge carrier extraction and significant charge recombination in the RPPSCs. Conversely, a PCP-Na HTL gives rise to highly crystalline and pinhole-free RPPSC films. Moreover, a PCP-Na HTL provides a better energy alignment at the perovskite/HTL interface because of its higher work function compared to PEDOT:PSS. Consequently, devices using PCP-Na as HTLs are more efficient in extracting charge carriers.

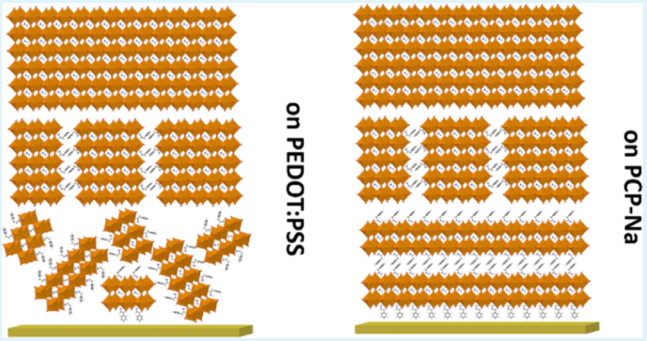

KEYWORDS: *Ruddlesden–Popper perovskite, orientation, phase composition, hole transport layer, morphology*

INTRODUCTION

Metal halide Ruddlesden–Popper perovskites (RPPs) are a class of perovskite-like materials described by the formula of $A'_2A_{n-1}B_nX_{3n+1}$, which consists of a large aromatic alkylammonium cation A′, a small organic cation A (methylammonium MA or formamidinium FA), a divalent metal cation B (lead or tin), and a halide anion X (Cl^-, Br^- or I^-).[1−7] The n value represents the thickness of the corner-sharing $[PbI_6]^{4-}$ octahedra layers capped by the bulky A′ cations.[5,8,9] The lower n members ($3 \leq n \leq 5$) of the RPP show much higher ambient stability than the pure three-dimensional (3D) perovskites. Therefore, they have been attracting increasing attention as light-absorbing materials in solar cells (SCs).[1,2,9−11] However, the power conversion efficiency (PCE) of this type of SC is still inferior to that of the pure 3D-based counterparts.

Early works on RPPSCs focused on manipulating the crystal structure of the RPP by varying the n numbers and the bulky A′ cations. Despite these efforts, RPPSCs showed very low short circuit current density (J_{SC}), fill factor (FF), and PCE (<5%), which are limited by the poor charge transport between the parallel-oriented inorganic octahedral layers isolated by the bulky cations.[1,2] In 2016, Tsai et al. reported the so-called hot-casting method that enabled the growth of vertically oriented RPP layers, with a consequent improvement of charge transport and PCE of the RPPSCs.[11] Later, alternative strategies, such as directly drop-cast film deposition method, solvent engineering, and the use of additives, have also been developed to grow vertically oriented RPP layers.[12−14] However, very little attention has been paid to how the different substrate materials on which the perovskite layer forms influence the orientation of the RPP layers. Only recently, Chen et al. suggested that the orientation of the inorganic octahedral layers of the RPP film is independent on the substrates due to the liquid–air nucleation and growth mechanism.[15]

The hole charge transport layer plays an important role in determining the charge extraction and recombination in the HPSCs.[16−20] Particularly, the bottom hole transport layer (HTL) affects not only the crystallinity but also the morphology of the perovskite film. Moreover, this layer influences the hole transfer and collection efficiency depending on the energy barrier at the HTL/perovskite interface and the

Received: March 21, 2020
Accepted: June 8, 2020
Published: June 8, 2020

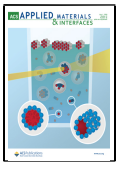

https://dx.doi.org/10.1021/acsami.0c05290
ACS Appl. Mater. Interfaces 2020, 12, 29505–29512

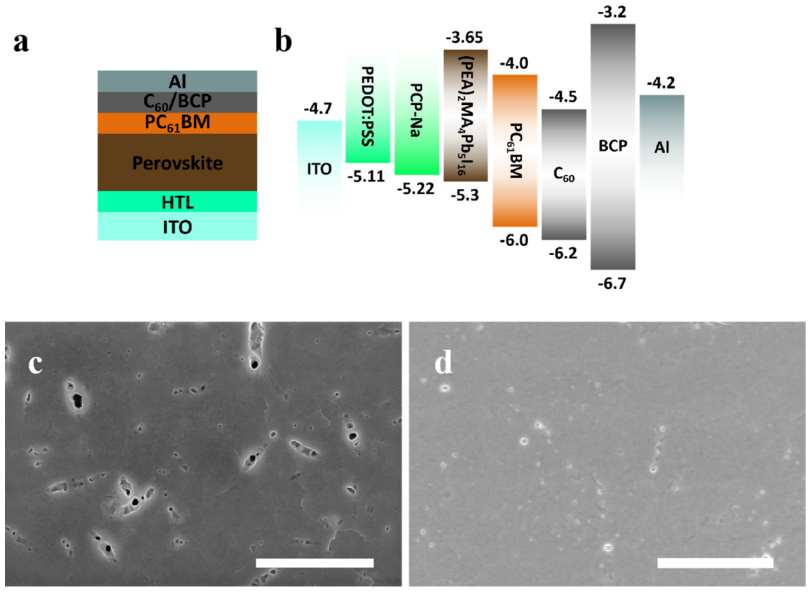

Figure 1. (a) Device structure and (b) energy level of each layer in the device structure. SEM images of RPP films on PEDOT:PSS (c) and PCP-Na (d) substrates; the scale-bar is 2 μm.

transport capability of the HTL. Poly(3,4-ethylenedioxythiophene) polystyrene sulfonate (PEDOT:PSS) is one of the most used HTLs in RPPSCs. Nevertheless, PEDOT:PSS has notorious drawbacks such as strong acidity, which causes corrosion to the ITO anode, determining a defective anode interface.[21] Moreover, perovskite films deposited on PEDOT:PSS are often noncompact and display a large number of pinholes, leading to high leakage and trap-assisted charge recombination losses in SCs.[16,22,23] In a recent work, we found that the deposition method and the solvents used for the precursor solution influence the quantity of the n = 2 phase, which is very crucial to the PCE of the RPP SCs.[9] Although we obtained higher efficiency by replacing the PEDOT:PSS with the PH neutral PCP-Na, we did not investigate the underlying reason for such improvement. Very recently, Chen et al. also reported higher performance in RPP SCs using the PCP-Na layer, and they simply attributed the higher efficiency to a better energy level matching at the interface.[24] However, whether other factors are contributing to the improvement remains unclear. In particular, we believe that the impact of the HTL on the orientation and quantity of the n = 2 phase is an important factor which deserves experimental investigation.

Herein, we aim to uncover the factors contributing to the performance difference of the RPPSCs using PEDOT:PSS and PCP-Na as HTLs. We systematically study how the HTLs affect the morphology, crystallinity, and orientation of the RPP films. When deposited on PEDOT:PSS, noncompact RPP films characterized by a large quantity of pinholes and structural defects probably due to its local anisotropic surface energy are obtained. However, on pH-neutral PCP-Na, compact RPP films could be deposited because of homogeneous surface energy for nucleation and growth. Both HTLs do not influence the orientation of the $n \geq 3$ phases; the inorganic layers are perpendicular to the substrate in the RPP films. They do, however, influence the orientation of the n = 2 phase, so that it is randomly oriented on PEDOT:PSS but is highly oriented on PCP-Na. The highly oriented and crystalline n = 2 phase on PCP-Na improves the crystallinity of the RPP film. Moreover, the PCP-Na HTL reduces the energy barrier at the perovskite/HTL interfaces. Therefore, the devices using PCP-Na HTLs are more efficient in extracting the charge carriers, resulting in a much higher PCE of 14.12% compared to 9.62% of the devices using PEDOT:PSS HTLs.

EXPERIMENTAL SECTION

Materials. PEDOT:PSS (Clevios VP AI 4083) was purchased from Heraeus. Perovskite precursor reagents such as PbI_2 (>99.99%), PEAI (phenylethylammonium iodide), and MAI (>98%) were acquired from TCI EUROPE N.V. The electron transport material PCBM was bought from Solenne BV. The electron transport material C60 (>99.9%), hole-blocking material BCP (99.99%), and solvent dimethylformamide (DMF) (99.8%) were acquired from Sigma-Aldrich. All the chemicals were used as received from the suppliers. PCP-Na was synthesized using a previously reported method.[25]

Device Fabrication and Characterization. In this work, the procedures for cleaning ITO glasses and depositing HTLs are the same as what we reported in a previous work.[9] We prepared the precursor solution of $PEA_2MA_4Pb_5I_{16}$ by dissolving PEAI, MAI, PbI_2, and NH_4SCN with a molar ratio of 2:4:5:2 in the DMF solvent, which has a concentration of 1.0 M for Pb^{2+}. We obtained $PEA_2MA_4Pb_5I_{16}$ films by spin-coating the precursor solution at 5000 rpm for 45 s and annealing at 100° for 10 min. Sequentially PCBM solution with a concentration of 20 mg mL^{-1} in chlorobenzene was spin-coated on top of the RPP films at 1000 rpm for 60 s. Then, C_{60}, BCP, and aluminum were deposited on top of PCBM, following the procedures used in our previous work.[9] J–V and external quantum efficiency measurements of the devices were obtained following the procedure reported previously.[9]

Perovskite Thin Film Characterization. Absorbance, X-ray diffraction (XRD), scanning electron microscopy (SEM), grazing incidence wide-angle X-ray scattering (GIWAXS), and photoluminescence (PL) measurements were performed following the procedure reported in our previous work.[9]

RESULTS AND DISCUSSION

Figure 1a shows the configuration of the RPPSCs, in which PEDOT:PSS and PCP-Na function as HTLs; the RPP film depicted by a nominal formula $(PEA)_2(MA)_4Pb_5I_{16}$ (n = 5) functions as the light-harvesting layer, and $PC_{61}BM/C_{60}$/BCP function as the electron transport layer (ETL). Figure 1b shows the energy level alignment at the interfaces of the

https://dx.doi.org/10.1021/acsami.0c05290
ACS Appl. Mater. Interfaces 2020, 12, 29505−29512

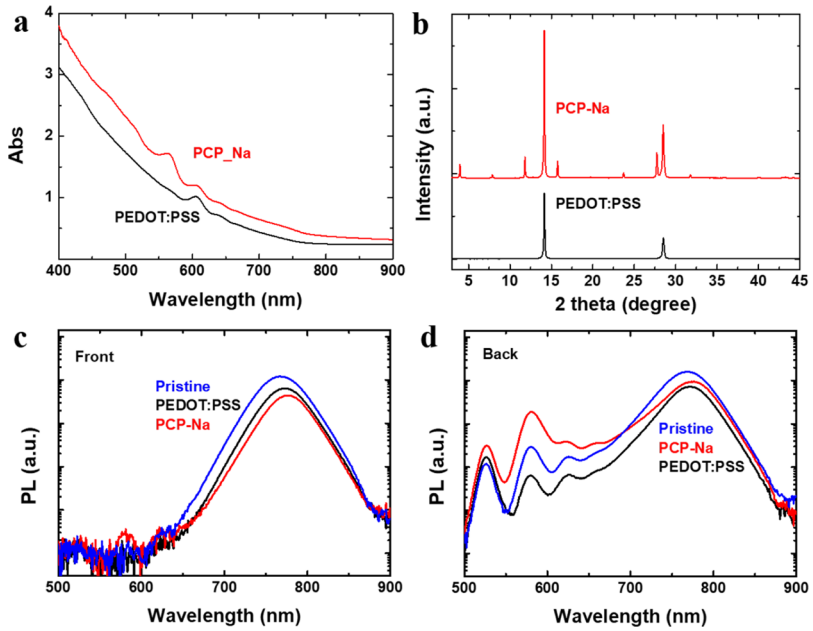

Figure 2. (a) Absorbance spectra, (b) XRD patterns, and semilogarithmic plot of steady state PL spectra excited from the (c) front and (d) back sides of the RPP films grown on PEDOT:PSS and PCP-Na.

RPPSCs, which is critical for charge transfer and extraction.[22,26] Compared to PEDOT:PSS, PCP-Na shows a reduced energy barrier at the perovskite/HTL interface because of its higher work function as shown in Figure 1b. This is beneficial to hole extraction and the built-in potential of the SC.

Figure 1c,d displays SEM images of the RPP films on the two HTLs. Apparently, the HTLs have a significant impact on the morphology of the RPP thin films. The RPP thin film on PEDOT:PSS forms a large quantity of pinholes with diameters ranging from several tens to several hundreds of nanometers. These pinholes can severely affect V_{OC} because the disrupted crystallinity around them can give rise to a large number of trap states and potentially cause significant trap-assisted charge recombination.[27−30] Moreover, they also cause high leakage current by creating shorts between the HTL and ETL. Overall, such a morphology is harmful for SC applications. In contrast, the RPP film grown on PCP-Na shows a negligible number of pinholes. Obviously, the surface energy of the HTLs determines the wetting properties of the perovskite solution, which in turn affects the nucleation and crystallization of the perovskite film. Macroscopically, PEDOT:PSS and PCP-Na layers are highly hydrophilic and enable good wetting of the RPP precursor solution on these HTLs. However, microscopic phase segregation happens between PEDOT and PSS.[31,32] We speculate that the local anisotropic wetting properties of PEDOT- and PSS-rich domains may cause nonuniform surface coverage. While for PCP-Na, the hydrophilic $-SO_3Na$ group is chemically bonded to the hydrophobic backbone, resulting in homogeneous wetting properties at a molecular level. This, we believe, provides an environment for uniform nucleation and subsequent crystallization and film growth, eliminating the pinholes effectively.

Figure 2a shows the absorbance spectra of the RPP films deposited on different HTLs. The absorption features at 514, 569, 605, 640, and 663 nm are attributed to the n = 1, 2, 3, 4, and 5 phases, respectively.[2,33] The RPP film on PEDOT:PSS does not show the obvious excitonic peak of the n = 2 phase, most probably because of its small quantity, while the RPP film on top of PCP-Na shows a stronger excitonic peak at 569 nm, indicating higher amounts of the n = 2 phase compared to that of films deposited on PEDOT:PSS.

Figure 2b shows the XRD patterns of RPP films grown on different HTLs. The two diffraction peaks coming from (110) and (220) planes of the RPP crystallites and located at 14.15 and 28.48° are more intense when PCP-Na is used as the HTL. This indicates that the RPP film on the PCP-Na layer has a much higher crystallinity than PEDOT:PSS. Moreover, the RPP film deposited on the PCP-Na layer exhibits obvious peaks of (00l) planes belonging to the n = 2 phase at 2θ = 3.96, 7.88, 11.82, and 15.82°. These peaks are not observable in the RPP film grown on PEDOT:PSS probably because of disordered packing and the noncrystalline nature of the n = 2 phase. The RPP films on both HTLs do not show any diffraction peaks of $5 \geq n \geq 3$ phases at $2\theta < 14.15°$. This is most probably due to the fact that these phases adopt the same orientation as the $n > 5$ phases, displaying two dominant peaks of (110) and (220) planes.

To gain more information about the phase composition and distribution in these RPP films, we collected the steady-state PL spectra of the RPP films on the two HTLs by illuminating a 400 nm pulsed laser on the perovskite films from the front and back side Figure 2c,d, respectively. Hereafter, we refer to the perovskite/air interface as the front side and the air/substrate interface as the back side. The RPP film has a high absorption coefficient of around 1.3×10^5 cm^{-1} at a wavelength of 400 nm, which has a penetration depth of about 33 nm into the RPP film. This means the excitation at the front side (back side) takes place mostly close to the top (bottom) part of the RPP films. The PL spectra recorded at the front side (Figures 2c and S1a) display only one peak (around 775 nm) from the 3D-like phase for both RPP films, suggesting that low-dimensional phases ($n \leq 7$) are less prevalently close to the top surface of these films. Interestingly, the main peak of the RPP film on top of PEDOT:PSS upon excitation from the front side is higher than for films on PCP-Na. The photogenerated carriers produced on the top part of the film

https://dx.doi.org/10.1021/acsami.0c05290
ACS Appl. Mater. Interfaces 2020, 12, 29505−29512

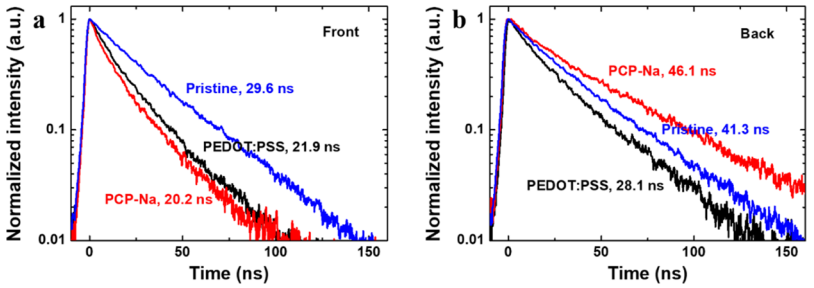

Figure 3. Time-resolved PL decay dynamics of the 3D-like phase of the RPP pristine film and films on PEDOT:PSS and PCP-Na layers excited from both sides by a 400 nm laser.

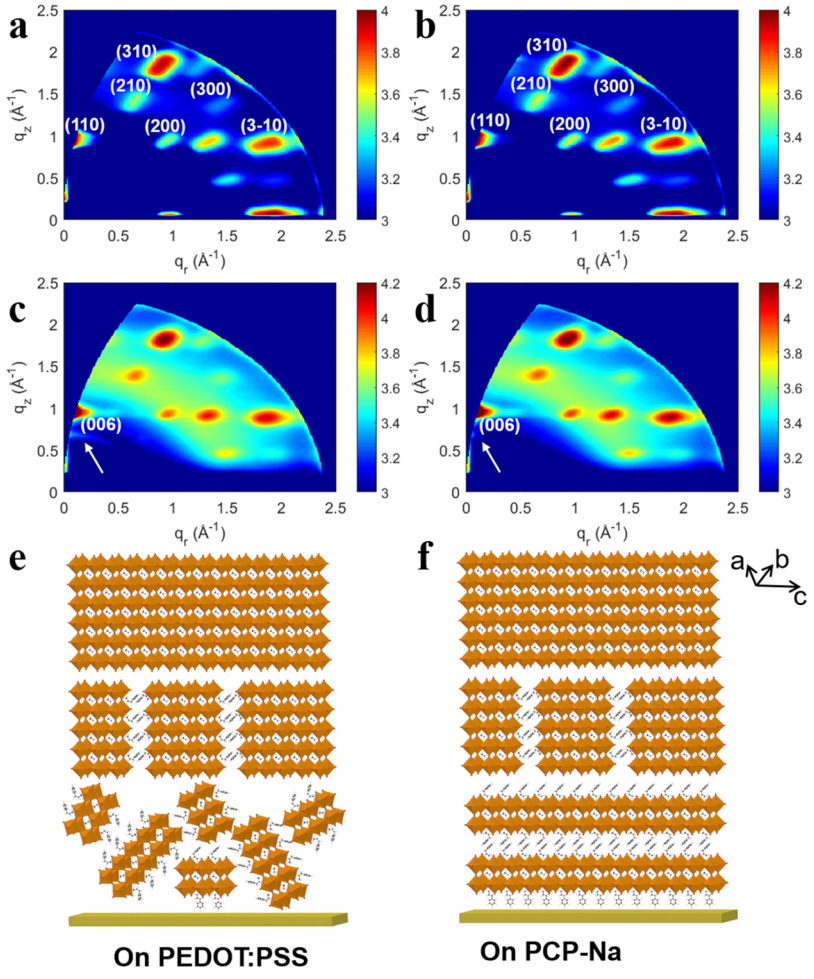

Figure 4. GIWAXS images and schematic illustration of RPP films on (a,c,e) PEDOT:PSS, (b,d,f) PCP-Na detected at 0.25 and 2.0°, respectively. The arrows indicate the diffraction signal of the (006) plane of the n = 2 phase.

undergo several processes in the presence of the HTL. First, some free charge carriers may recombine with each other radiatively. Second, some other free charge carriers may be captured by the trap sites and recombine nonradiatively. Third, some of the charge carriers diffuse away from the excitation region. Because the top surface is far from the bottom interface, the crystallinity of the sample plays an important role on the diffusion length.[34,35] Therefore, in case of PCP-Na, more charge carriers diffuse away from the top surface because of the higher packing order of the film, reducing the carrier density on the top part of the film and possibility of the radiative recombination process. In case of the samples on PEDOT:PSS, this channel is cut by the disorder, and therefore, the probability of charge recombination from the bulk is higher. This landscape is in agreement with a much higher PL intensity measured on a glass substrate, where namely, besides surface defects, there is no other sink for photoexcitations.

The PL spectra recorded on the back side exhibit not only emission from the 3D-like phase but also weak emission from the $n \leq 7$ phases (Figures 2d and S1b). These results demonstrate the graded vertical phase distribution in the RPP films on both HTLs, where the low-dimensional phases preferentially stay at the bottom.

Upon back excitation, the charge carriers are generated close to the perovskite/HTL interface. The charge carriers on both RPP films can diffuse very efficiently to the perovskite/HTL

https://dx.doi.org/10.1021/acsami.0c05290
ACS Appl. Mater. Interfaces 2020, 12, 29505−29512

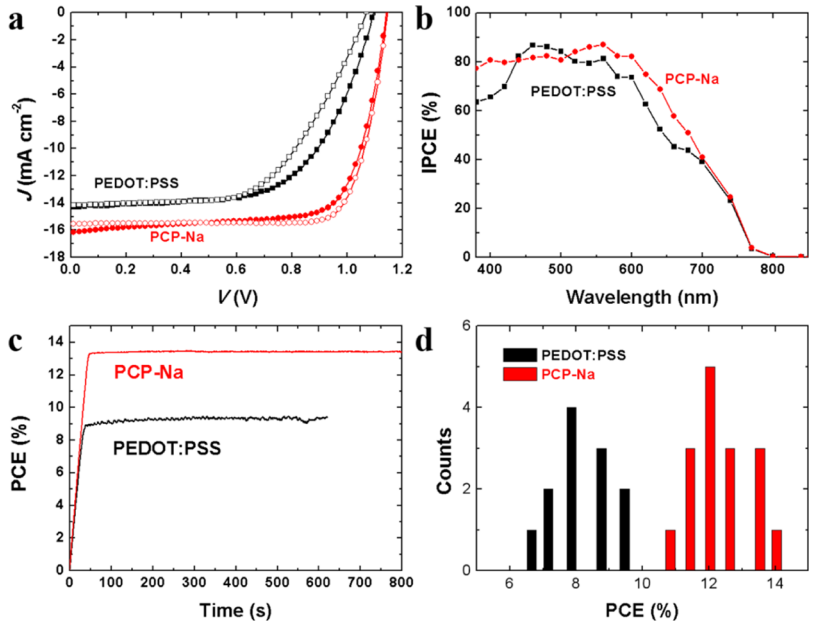

Figure 5. (a) $J-V$ curves, (b) external quantum efficiency spectra, (c) steady-state PCE tracked at a maximum power point, and (d) the statistics of the PCE for the devices using PEDOT:PSS and PCP-Na HTLs.

interface. Now that the diffusion is not hindered but there is lack of crystallinity, and the trap states at the interface play a more important role. As the RPP film on PCP-Na has a much lower trap density, the nonradiative recombination is considerably lower, leading to higher radiative charge recombination. A further enhancement in the PL signal for the PCP-Na sample is probably due to the energy transfer from the low-dimensional phases present at the bottom of the sample toward the bulk perovskite.

This is also evident from the comparison of the time-resolved PL decay dynamics (see Figure 3) of the 3D-like phase in the RPP perovskite films deposited on glass and HTLs. The extremely low exciton binding energy of the 3D-like phases enables free charge carriers to be the dominant photoexcited species at room temperature.[36−39] Upon front excitation, the RPP films on both PEDOT:PSS and PCP-Na exhibit faster PL decay dynamics than the RPP film on glass, leading to a shorter charge carrier lifetime. As we mentioned previously, the three processes, such as recombination of free charge carriers, recombination of the hole (electron) with trapped electrons (hole), and diffusion of the charge carriers and subsequent hole transfer at the perovskite/HTL interface, reduce the lifetime of these free charge carriers in the RPP films. The recombination of free holes and electrons is higher in the RPP film on PEDOT:PSS compared to that on PCP-Na, while the quantity of holes transferred to the HTL is larger in the RPP film on PCP-Na than that on PEDOT:PSS.

In general, the excitation at the back side produces a longer charge carrier lifetime in RPP films compared to the excitation from the front side because of energy transfer from low-dimensional phases to the 3D-like phase. Unlike the excitation at the front side, the PL decay of the RPP film on PEDOT:PSS is much faster than that of the RPP film on PCP-Na because of severe trap-mediated charge recombination. Conversely, the compact and highly crystalline RPP film on PCP-Na gives rise to long-lived charge carriers because of reduced charge recombination. These results are consistent with our observation in steady-state PL spectra.

We conducted GIWAXS experiments at incident angles (α_i) of 0.25 and 2° (Figure 4) to further investigate how the HTLs affect the orientation of the perovskite phases. Independent on the X-ray penetration depth, the RPP films on both HTLs show sharp Bragg spots at $q_z \approx 1.0$ Å^{-1}, which could be indexed to be (110) planes of the $n \geq 3$ phases, packing in the out-of-plane direction.[8,13] This means that the inorganic slabs of $n \geq 3$ phases are perpendicular to the substrate. The Bragg spot at $q_r \approx 1.0$ Å^{-1} assigned to the in-plane-oriented (110) planes is much weaker, confirming the dominant vertical orientation of the $n \geq 3$ phases. When X-rays penetrate the entire film ($\alpha_i = 2°$), very weak diffraction features appear at $q_z \approx 0.85$ A^{-1} in the RPP films, which is indexed to be the (006) plane of the $n = 2$ phase, and is absent in the case of the shallow X-ray penetration depth ($\alpha_i = 0.25°$). These results confirm that there is a very little $n = 2$ phase, and at the same time, they corroborate the notion that the two-dimensional (2D) phases preferentially crystallize at the bottom of the film. Compared to the high n members, the orientation of the $n = 2$ phase has a much stronger dependence on the HTLs. The diffraction spot indicates a highly oriented $n = 2$ phase with the $[PbI_6]^{4-}$ layer parallel to the substrate on the top of PCP-Na, while the diffraction arc represents the randomly oriented $n = 2$ phase in the RPP film on PEDOT:PSS. The line cut plots in the out-of-plane and in-plane direction further confirm our observation here (Figure S2). The highly oriented and crystalline nature of the $n = 2$ phase in the RPP film on top of PCP-Na indicates that the $n = 2$ phase segregates into domains. Because the 3D-like phase component is dominant in the RPP film, the $n = 2$ phase forms small segregated domains embedded in the 3D-like phase, which do not hinder the charge transport and extraction.[40] Moreover, the highly crystalline $n \geq 3$ phases in the RPP film on top of PCP-Na facilitate the charge transport. Conversely, the randomly oriented and noncrystalline $n = 2$ phase in the RPP film on top of PEDOT:PSS is distributed more uniformly in the 3D-like phase without obvious segregation, which creates energy disorder for charge transport. The less crystalline $n \geq 3$ phases

https://dx.doi.org/10.1021/acsami.0c05290
ACS Appl. Mater. Interfaces 2020, 12, 29505−29512

in the RPP film on top of PEDOT:PSS are also unfavorable for charge transport.

In one of our recent works, we found that the parallel-oriented 2D (n = 2) tin perovskite induces the formation of highly oriented and crystalline 3D tin perovskites.[5] The *in situ* GIWAXS experiments proved that the suppressed bulk crystallization of the 3D phase in the presence of these highly oriented n = 2 phase tin perovskites is responsible for its stronger crystallinity and orientation.[41] The same mechanism may apply to the RPP films investigated in this work. Therefore, we conclude that the larger amount of the highly ordered n = 2 phase is favorable for highly crystalline $n \geq 3$ phases in the RPP film on the PCP-Na HTL.

Figure 5a shows the $J-V$ curves under illumination of the champion SCs using the two HTLs, and Table 1 summarizes the performance parameters. The device using PEDOT:PSS as the HTL shows a V_{OC} of 1.09 (1.07) V, a J_{SC} of 14.30 (14.16) mA cm^{-2}, a FF of 0.61 (0.58), and a PCE of 9.62% (8.76%), when measured in the forward (reverse) direction, respectively. Devices using PCP-Na as the HTL have superior performance, that is, a V_{OC} of 1.15 (1.14) V, a J_{SC} of 15.54 (16.17) mA cm^{-2}, an FF of 0.79 (0.72), and a PCE of 14.12% (13.35%) in the forward (reverse) scan. The PCEs of these two devices recorded at a maximum power point are stable over time and show very close numbers to those obtained from the $J-V$ curves (Figure 5c). Figure 5b shows the external quantum efficiency spectra of the different SCs, which give rise to an integrated current density of 15.97 and 14.70 mA cm^{-2} for PCP-Na and PEDOT: PSS SCs, respectively. These values verify the J_{SC} obtained from $J-V$ curves. The statistical distribution of the PCE (Figure 5d) measured over more than 10 devices for each HTL consistently proves the superior performance of the device using the PCP-Na HTL. The severe trap-mediated charge recombination and recombination of the free electrons and holes leads to bigger hysteresis and lower PCE of the PEDOT:PSS device. In contrast, the reduced charge recombination in PCP-Na-based devices leads to a much higher device performance.

Table 1. Performance Parameters of the Devices Using PEDOT:PSS and PCP-Na HTLs

device	V_{OC} (V)	J_{SC} (mA cm^{-2})	FF	PCE (%)
PEDOT:PSS	1.09	14.30	0.61	9.62
	1.07	14.16	0.58	8.76
PCP-Na	1.15	15.54	0.79	14.12
	1.14	16.17	0.72	13.35

In order to study the charge recombination in SCs using different HTLs, we monitored the variation in J_{SC} and V_{OC} when devices are exposed to different light intensities (I). In the logarithmic plot of J_{SC} as a function of I (see Figure 6a), the device using PEDOT:PSS exhibits a slope much lower than one (0.82), confirming significant recombination of free holes and electrons because of inefficient charge transport and extraction. As discussed previously, the low crystalline 3D perovskite phase and disordered n = 2 phase could be the main factors inhibiting the charge transport. The pileup of the free charge carriers increases their recombination. Conversely, the PCP-Na device has a much steeper slope (0.95), confirming the reduced recombination of free charge carriers. This is attributed to more efficient charge transport in the highly crystalline RPP film and hole extraction at the perovskite/PCP-Na interface. Similarly, this explains the improved current density and FF of the PCP-Na-based devices. Figure 6b shows the light intensity dependence of V_{OC} of these two devices. The PEDOT:PSS-based device has a steep slope (1.93 kT/q), indicating severe trap-mediated charge recombination losses. While the PCP-Na-based device has a much shallower slope (1.35 kT/q), indicating a considerably reduced trap-mediated charge recombination loss. These results are fully consistent with the transient PL data and explain the difference in the performance of the SCs fabricated on the two investigated HTLs.

CONCLUSIONS

In conclusion, we studied how the HTL impacts film quality and charge extraction in the RPPSCs. We compared the crystallinity and phase purity of RPP films grown on top of two different HTLs, namely PEDOT:PSS and PCP-Na. When PEDOT:PSS is used as the HTL, the RPP films are of lower crystallinity and exhibit large pinholes. In addition, PEDOT:PSS induces the random orientation of the n = 2 phase at the perovskite/PEDOT:PSS interface. These factors create significant trap-assisted and free charge carrier recombination, leading to poor charge carrier extraction and low PCE. Conversely, PCP-Na gives rise to highly crystalline and compact RPP films. The order of the n = 2 phase at the HTL interface is instrumental to obtain the high degree of crystallinity. Consequently, PCP-Na extracts the charge carriers more efficiently, resulting in a significant improvement (up to 14.12%) of the PCE.

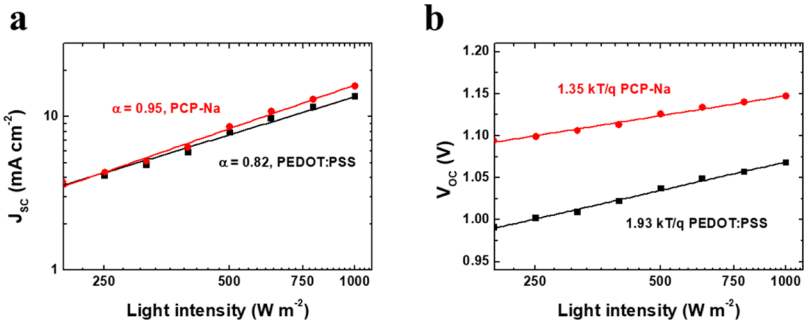

Figure 6. Light intensity dependence of J_{SC} (a) and V_{OC} (b) of the devices using PEDOT:PSS and PCP-Na HTLs.

https://dx.doi.org/10.1021/acsami.0c05290
ACS Appl. Mater. Interfaces 2020, 12, 29505−29512

■ ASSOCIATED CONTENT

Supporting Information

The Supporting Information is available free of charge at https://pubs.acs.org/doi/10.1021/acsami.0c05290.

Linear plots of steady-state PL spectra and line-cut plots in different directions of GIWAXS measurements (PDF)

■ AUTHOR INFORMATION

Corresponding Authors

Shuyan Shao − *Zernike Institute for Advanced Materials, University of Groningen, Groningen 9747 AG, The Netherlands*; Email: S.Shao@rug.nl

Maria A. Loi − *Zernike Institute for Advanced Materials, University of Groningen, Groningen 9747 AG, The Netherlands*; orcid.org/0000-0002-7985-7431; Email: M.A.Loi@rug.nl

Authors

Qingqian Wang − *Zernike Institute for Advanced Materials, University of Groningen, Groningen 9747 AG, The Netherlands; Photonics and Optoelectronics Lab, Department of Physics, University of Cagliari, Monserrato I-09042, Italy*

Bowei Xu − *Beijing National Laboratory for Molecular Sciences, Institute of Chemistry, Chinese Academy of Sciences, Beijing 100190, China*; orcid.org/0000-0001-6467-6147

Herman Duim − *Zernike Institute for Advanced Materials, University of Groningen, Groningen 9747 AG, The Netherlands*

Jingjin Dong − *Zernike Institute for Advanced Materials, University of Groningen, Groningen 9747 AG, The Netherlands*

Sampson Adjokatse − *Zernike Institute for Advanced Materials, University of Groningen, Groningen 9747 AG, The Netherlands*

Giuseppe Portale − *Zernike Institute for Advanced Materials, University of Groningen, Groningen 9747 AG, The Netherlands*; orcid.org/0000-0002-4903-3159

Jianhui Hou − *Beijing National Laboratory for Molecular Sciences, Institute of Chemistry, Chinese Academy of Sciences, Beijing 100190, China*; orcid.org/0000-0002-2105-6922

Michele Saba − *Photonics and Optoelectronics Lab, Department of Physics, University of Cagliari, Monserrato I-09042, Italy*; orcid.org/0000-0001-6416-3122

Complete contact information is available at: https://pubs.acs.org/10.1021/acsami.0c05290

Notes

The authors declare no competing financial interest.

■ ACKNOWLEDGMENTS

This work is partially financed by the Netherlands Organization for Scientific Research (NWO). This is a publication of the FOM-focus Group "Next Generation Organic Photovoltaics," participating in the Dutch Institute for Fundamental Energy Research (DIFFER). B.X. acknowledges the financial support from the Natural Science Foundation of China (grant no. 21875263). The authors like to thank Arjen Kamp and Teo Zaharia for their help in solving technical problems in the laboratory.

■ REFERENCES

(1) Smith, I. C.; Hoke, E. T.; Solis-Ibarra, D.; McGehee, M. D.; Karunadasa, H. I. A Layered Hybrid Perovskite Solar-Cell Absorber with Enhanced Moisture Stability. *Angew. Chem., Int. Ed.* **2014**, *53*, 11232−11235.

(2) Cao, D. H.; Stoumpos, C. C.; Farha, O. K.; Hupp, J. T.; Kanatzidis, M. G. 2D Homologous Perovskites as Light-Absorbing Materials for Solar Cell Applications. *J. Am. Chem. Soc.* **2015**, *137*, 7843−7850.

(3) Stoumpos, C. C.; Cao, D. H.; Clark, D. J.; Young, J.; Rondinelli, J. M.; Jang, J. I.; Hupp, J. T.; Kanatzidis, M. G. Ruddlesden−Popper Hybrid Lead Iodide Perovskite 2D Homologous Semiconductors. *Chem. Mater.* **2016**, *28*, 2852−2867.

(4) Calabrese, J.; Jones, N. L.; Harlow, R. L.; Herron, N.; Thorn, D. L.; Wang, Y. Preparation and Characterization of Layered Lead Halide Compounds. *J. Am. Chem. Soc.* **1991**, *113*, 2328−2330.

(5) Shao, S.; Liu, J.; Portale, G.; Fang, H.; Blake, G. R.; ten Brink, G. H.; Koster, L. J. A.; Loi, M. A. Highly Reproducible Sn-based Hybrid Perovskite Solar Cells with 9% Efficiency. *Adv. Energy Mater.* **2018**, *8*, 1702019.

(6) Milot, R. L.; Sutton, R. J.; Eperon, G. E.; Haghighirad, A. A.; Martinez Hardigree, J.; Miranda, L.; Snaith, H. J.; Johnston, M. B.; Herz, L. M. Charge-Carrier Dynamics in 2D Hybrid Metal−Halide Perovskites. *Nano Lett.* **2016**, *16*, 7001−7007.

(7) Yang, J.; Zuo, C.; Peng, Y.; Yang, Y.; Yang, X.; Ding, L. Large-Area Perovskite Solar Cells. *Sci. Bull.* **2020**, *65*, 872−875.

(8) Shao, S.; Dong, J.; Duim, H.; ten Brink, G. H.; Blake, G. R.; Portale, G.; Loi, M. A. Enhancing the Crystallinity and Perfecting the Orientation of Formamidinium Tin Iodide for Highly Efficient Sn-Based Perovskite Solar Cells. *Nano Energy* **2019**, *60*, 810−816.

(9) Shao, S.; Duim, H.; Wang, Q.; Xu, B.; Dong, J.; Adjokatse, S.; Blake, G. R.; Protesescu, L.; Portale, G.; Hou, J.; Saba, M.; Loi, M. A. Tuning the Energetic Landscape of Ruddlesden−Popper Perovskite Films for Efficient Solar Cells. *ACS Energy Lett.* **2019**, *5*, 39−46.

(10) Proppe, A. H.; Quintero-Bermudez, R.; Tan, H.; Voznyy, O.; Kelley, S. O.; Sargent, E. H. Synthetic Control over Quantum Well Width Distribution and Carrier Migration in Low-Dimensional Perovskite Photovoltaics. *J. Am. Chem. Soc.* **2018**, *140*, 2890−2896.

(11) Tsai, H.; Nie, W.; Blancon, J.-C.; Stoumpos, C. C.; Asadpour, R.; Harutyunyan, B.; Neukirch, A. J.; Verduzco, R.; Crochet, J. J.; Tretiak, S.; Pedesseau, L.; Even, J.; Alam, M. A.; Gupta, G.; Lou, J.; Ajayan, P. M.; Bedzyk, M. J.; Kanatzidis, M. G.; Mohite, A. D. High-Efficiency Two-Dimensional Ruddlesden−Popper Perovskite Solar Cells. *Nature* **2016**, *536*, 312−316.

(12) Zuo, C.; Scully, A. D.; Vak, D.; Tan, W.; Jiao, X.; McNeill, C. R.; Angmo, D.; Ding, L.; Gao, M. Self-Assembled 2D Perovskite Layers for Efficient Printable Solar Cells. *Adv. Energy Mater.* **2019**, *9*, 1803258.

(13) Ma, C.; Lo, M.-F.; Lee, C.-S. A Simple Method for Phase Control in Two-Dimensional Perovskite Solar Cells. *J. Mater. Chem. A* **2018**, *6*, 18871−18876.

(14) Qing, J.; Liu, X.-K.; Li, M.; Liu, F.; Yuan, Z.; Tiukalova, E.; Yan, Z.; Duchamp, M.; Chen, S.; Wang, Y.; Bai, S.; Liu, J.-M.; Snaith, H. J.; Lee, C.-S.; Sum, T. C.; Gao, F. Aligned and Graded Type-II Ruddlesden−Popper Perovskite Films for Efficient Solar Cells. *Adv. Energy Mater.* **2018**, *8*, 1800185.

(15) Chen, A. Z.; Shiu, M.; Ma, J. H.; Alpert, M. R.; Zhang, D.; Foley, B. J.; Smilgies, D.-M.; Lee, S.-H.; Choi, J. J. Origin of Vertical Orientation in Two-Dimensional Metal Halide Perovskites and Its Effect on Photovoltaic Performance. *Nat. Commun.* **2018**, *9*, 1336.

(16) Shao, S.; Loi, M. A. The Role of the Interfaces in Perovskite Solar Cells. *Adv. Mater. Interfaces* **2020**, *7*, 1901469.

(17) Bi, C.; Wang, Q.; Shao, Y.; Yuan, Y.; Xiao, Z.; Huang, J. Non-Wetting Surface-Driven High-Aspect-Ratio Crystalline Grain Growth for Efficient Hybrid Perovskite Solar Cells. *Nat. Commun.* **2015**, *6*, 7747.

(18) Serpetzoglou, E.; Konidakis, I.; Kakavelakis, G.; Maksudov, T.; Kymakis, E.; Stratakis, E. Improved Carrier Transport in Perovskite Solar Cells Probed by Femtosecond Transient Absorption Spectroscopy. *ACS Appl. Mater. Interfaces* **2017**, *9*, 43910−43919.

(19) Fang, Z.; Meng, X.; Zuo, C.; Li, D.; Xiao, Z.; Yi, C.; Wang, M.; Jin, Z.; Yang, S.; Ding, L. Interface Engineering Gifts CsPbI2. 25Br0. 75 Solar Cells High Performance. *Sci. Bull.* **2019**, *64*, 1743−1746.

(20) Zuo, C.; Ding, L. Modified PEDOT Layer Makes a 1.52 V Voc for Perovskite/PCBM Solar Cells. *Adv. Energy Mater.* **2017**, *7*, 1601193.
(21) Shao, S.; Liu, J.; Bergqvist, J.; Shi, S.; Veit, C.; Würfel, U.; Xie, Z.; Zhang, F. In Situ Formation of MoO3 in PEDOT: PSS Matrix: A Facile Way to Produce a Smooth and Less Hygroscopic Hole Transport Layer for Highly Stable Polymer Bulk Heterojunction Solar Cells. *Adv. Energy Mater.* **2013**, *3*, 349−355.
(22) Shao, S.; Cui, Y.; Duim, H.; Qiu, X.; Dong, J.; ten Brink, G. H.; Portale, G.; Chiechi, R. C.; Zhang, S.; Hou, J.; Loi, M. A. Enhancing the Performance of the Half Tin and Half Lead Perovskite Solar Cells by Suppression of the Bulk and Interfacial Charge Recombination. *Adv. Mater.* **2018**, *30*, 1803703.
(23) Adjokatse, S.; Kardula, J.; Fang, H. H.; Shao, S.; ten Brink, G. H.; Loi, M. A. Effect of the Device Architecture on the Performance of FA0. 85MA0. 15PbBr0. 45I2. 55 Planar Perovskite Solar Cells. *Adv. Mater. Interfaces* **2019**, *6*, 1801667.
(24) Lian, X.; Chen, J.; Zhang, Y.; Tian, S.; Qin, M.; Li, J.; Andersen, T. R.; Wu, G.; Lu, X.; Chen, H. Two-Dimensional Inverted Planar Perovskite Solar Cells with Efficiency over 15% via Solvent and Interface Engineering. *J. Mater. Chem. A* **2019**, *7*, 18980−18986.
(25) Cui, Y.; Xu, B.; Yang, B.; Yao, H.; Li, S.; Hou, J. A Novel PH Neutral Self-Doped Polymer for Anode Interfacial Layer in Efficient Polymer Solar Cells. *Macromolecules* **2016**, *49*, 8126−8133.
(26) Zhang, X.; Wu, G.; Fu, W.; Qin, M.; Yang, W.; Yan, J.; Zhang, Z.; Lu, X.; Chen, H. Orientation Regulation of Phenylethylammonium Cation Based 2D Perovskite Solar Cell with Efficiency Higher than 11%. *Adv. Energy Mater.* **2018**, *8*, 1702498.
(27) Shao, S.; Abdu-Aguye, M.; Sherkar, T. S.; Fang, H.-H.; Adjokatse, S.; Brink, G. t.; Kooi, B. J.; Koster, L. J. A.; Loi, M. A. The Effect of the Microstructure on Trap-assisted Recombination and Light Soaking Phenomenon in Hybrid Perovskite Solar Cells. *Adv. Funct. Mater.* **2016**, *26*, 8094−8102.
(28) de Quilettes, D. W.; Vorpahl, S. M.; Stranks, S. D.; Nagaoka, H.; Eperon, G. E.; Ziffer, M. E.; Snaith, H. J.; Ginger, D. S. Impact of Microstructure on Local Carrier Lifetime in Perovskite Solar Cells. *Science* **2015**, *348*, 683−686.
(29) Shao, S.; Abdu-Aguye, M.; Qiu, L.; Lai, L.-H.; Liu, J.; Adjokatse, S.; Jahani, F.; Kamminga, M. E.; ten Brink, G. H.; Palstra, T. T. M.; Kooi, B. J.; Hummelen, J. C.; Antonietta Loi, M. Elimination of the Light Soaking Effect and Performance Enhancement in Perovskite Solar Cells Using a Fullerene Derivative. *Energy Environ. Sci.* **2016**, *9*, 2444−2452.
(30) Liu, J.; Lu, S.; Zhu, L.; Li, X.; Choy, W. C. H. Perovskite-Organic Hybrid Tandem Solar Cells Using a Nanostructured Perovskite Layer as the Light Window and a PFN/Doped-MoO 3/MoO 3 Multilayer as the Interconnecting Layer. *Nanoscale* **2016**, *8*, 3638−3646.
(31) Nardes, A. M.; Kemerink, M.; Janssen, R. A. J.; Bastiaansen, J. A. M.; Kiggen, N. M. M.; Langeveld, B. M. W.; van Breemen, A. J. J. M.; de Kok, M. M. Microscopic Understanding of the Anisotropic Conductivity of PEDOT: PSS Thin Films. *Adv. Mater.* **2007**, *19*, 1196−1200.
(32) Higgins, A. M.; Martin, S. J.; Jukes, P. C.; Geoghegan, M.; Jones, R. A. L.; Langridge, S.; Cubitt, R.; Kirchmeyer, S.; Wehrum, A.; Grizzi, I. Interfacial Structure in Semiconducting Polymer Devices. *J. Mater. Chem.* **2003**, *13*, 2814−2818.
(33) Quan, L. N.; Yuan, M.; Comin, R.; Voznyy, O.; Beauregard, E. M.; Hoogland, S.; Buin, A.; Kirmani, A. R.; Zhao, K.; Amassian, A.; Kim, D. H.; Sargent, E. H. Ligand-Stabilized Reduced-Dimensionality Perovskites. *J. Am. Chem. Soc.* **2016**, *138*, 2649−2655.
(34) Ciesielski, R.; Schäfer, F.; Hartmann, N. F.; Giesbrecht, N.; Bein, T.; Docampo, P.; Hartschuh, A. Grain Boundaries Act as Solid Walls for Charge Carrier Diffusion in Large Crystal MAPI Thin Films. *ACS Appl. Mater. Interfaces* **2018**, *10*, 7974−7981.
(35) Xie, F. X.; Su, H.; Mao, J.; Wong, K. S.; Choy, W. C. H. Evolution of Diffusion Length and Trap State Induced by Chloride in Perovskite Solar Cell. *J. Phys. Chem. C* **2016**, *120*, 21248−21253.
(36) Shang, Q.; Wang, Y.; Zhong, Y.; Mi, Y.; Qin, L.; Zhao, Y.; Qiu, X.; Liu, X.; Zhang, Q. Unveiling Structurally Engineered Carrier Dynamics in Hybrid Quasi-Two-Dimensional Perovskite Thin Films toward Controllable Emission. *J. Phys. Chem. Lett.* **2017**, *8*, 4431−4438.
(37) Even, J.; Pedesseau, L.; Katan, C. Analysis of Multivalley and Multibandgap Absorption and Enhancement of Free Carriers Related to Exciton Screening in Hybrid Perovskites. *J. Phys. Chem. C* **2014**, *118*, 11566−11572.
(38) Fang, H.-H.; Raissa, R.; Abdu-Aguye, M.; Adjokatse, S.; Blake, G. R.; Even, J.; Loi, M. A. Photophysics of Organic−Inorganic Hybrid Lead Iodide Perovskite Single Crystals. *Adv. Funct. Mater.* **2015**, *25*, 2378−2385.
(39) Miyata, A.; Mitioglu, A.; Plochocka, P.; Portugall, O.; Wang, J. T.-W.; Stranks, S. D.; Snaith, H. J.; Nicholas, R. J. Direct Measurement of the Exciton Binding Energy and Effective Masses for Charge Carriers in Organic−Inorganic Tri-Halide Perovskites. *Nat. Phys.* **2015**, *11*, 582−587.
(40) van Reenen, S.; Kemerink, M.; Snaith, H. J. Modeling Anomalous Hysteresis in Perovskite Solar Cells. *J. Phys. Chem. Lett.* **2015**, *6*, 3808−3814.
(41) Dong, J.; Shao, S.; Kahmann, S.; Rommens, A. J.; Hermida-Merino, D.; ten Brink, G. H.; Loi, M. A.; Portale, G. Mechanism of Crystal Formation in Ruddlesden−Popper Sn-Based Perovskites. *Adv. Funct. Mater.* **2020**, *30*, 2001294.

https://dx.doi.org/10.1021/acsami.0c05290
ACS Appl. Mater. Interfaces 2020, 12, 29505−29512